Calculating the inverse Hessian

Now that we have found the forward operators that separately balance amplitude and frequency content from $\mathbf{m}_0$ to $\mathbf{m_1}$, where $\mathbf{m}_1 \approx \mathbf{H}\mathbf{m}_0$, we want to find what combination of $\mathbf{A}$ and $\mathbf{S}$ best approximates $\mathbf{H}$. Since $\mathbf{H} = \mathbf{L}^\mathsf{T}\mathbf{L}$ is symmetric, we want our approximation of $\mathbf{H}$ to be as close to symmetric as possible. Therefore, we define $\mathbf{H}$ as

$$\mathbf{H} \approx \mathbf{A}^{1/2}\mathbf{S}\mathbf{A}^{1/2} \,, \tag{5.9}$$

where $\mathbf{A}$ is the operator that balances the amplitudes of $\mathbf{m}_0$ with respect to $\mathbf{m}_1$, and $\mathbf{S}$ is the operator that balances the local frequency content of $\mathbf{m}_0$ with respect to $\mathbf{m}_1$, both defined previously. Applying the operations in this order allows the approximation of $\mathbf{H}$ to be symmetric because both $\mathbf{A}$ and $\mathbf{S}$ are symmetric operations. Splitting up our approximation to the Hessian into two separate operators allows us to control how much of each operation and the order of each operation goes into correcting the image, and see how it affects the resulting image. Now that we have found the forward Hessian, $\mathbf{H}$, such that $\mathbf{H}\mathbf{m}_0 \approx \mathbf{m}_1$ using data matching operators, we want to find the inverse of this operator, $\mathbf{H}^{-1}$, such that $\hat{\mathbf{r}} \approx \mathbf{H}^{-1}\mathbf{m}_0$ provides us with the least-squares image. This is found as

$$\mathbf{H}^{-1} \approx \left(\mathbf{A}^{1/2}\mathbf{S}\mathbf{A}^{1/2}\right)^{-1} = \mathbf{A}^{-1/2}\mathbf{S}^{-1}\mathbf{A}^{-1/2} \,. \tag{5.10}$$

Because the amplitude operators only contain diagonal terms, they are simple to invert. However, $\mathbf{S}^{-1}$ is non-trivial to calculate since inverse smoothing can create physically unrealistic high-frequency data if inverted incorrectly without regularization.

Figure 5.4 shows transfer functions for a stationary forward and inverse triangle smoothing operator of a radius of 10 samples. In the forward case, triangle

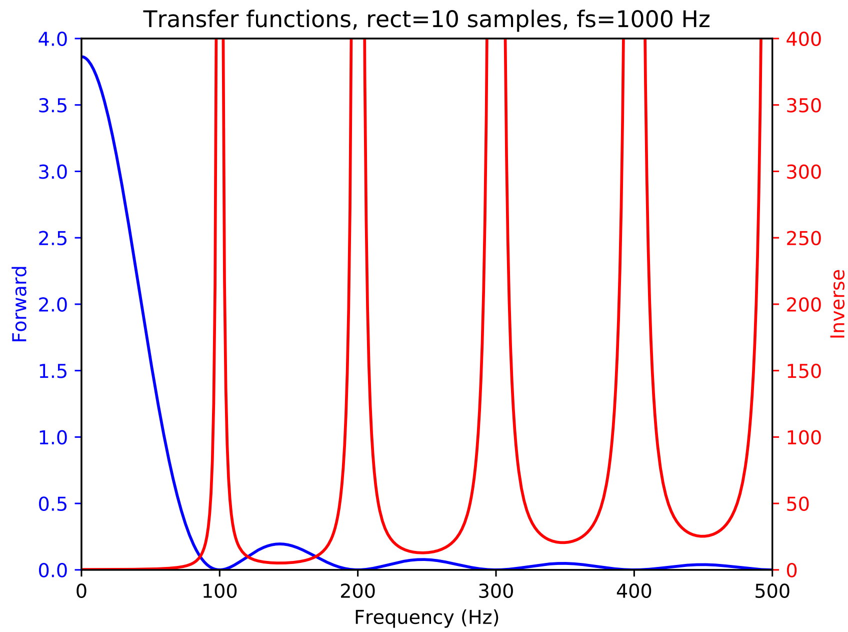

Figure 5.4: Transfer functions for a stationary forward triangle smoothing operator (blue) and its inverse (red). $\boxed{\text{chapter-mighes/triop tf}}$

smoothing acts as a low-pass filter. However, its inverse can introduce high frequency information, which is physically unrealistic for the data we are working with.

Therefore, $\mathbf{S}^{-1}$ must be calculated with care to ensure the inverted data is physically plausible. We iteratively invert $\mathbf{S}$ using shaping regularization (Fomel, 2007b), where the shaping operator is a bandpass filter picked to ensure the passband contains only physically possible frequencies for the given data set. The cost of applying our approximation to $\mathbf{H}^{-1}$ in equation (5.10) is $\mathcal{O}(N)$, where N is the image size. The constant is small, typically around 10 for the number of iterations, and the calculation and application of this approximation is computationally insignificant compared to one iteration of least-squares migration.

EXAMPLE

We demonstrate the effectiveness of this method on the 2D Sigsbee model. The Sigsbee2A 2D synthetic data set was created to mimic the geology of the Sigsbee escarpment in the Gulf of Mexico (Paffenholz et al., 2002). A fixed-spread acquisition survey is generated, which consists of 301 shots spaced every 122 m. The source wavelet for generating the synthetic data is a Ricker wavelet centered at 10 Hz. The record length of the synthetic data is 10 s with a sampling interval of 4 ms. We use reverse-time migration (RTM) as our migration operator.

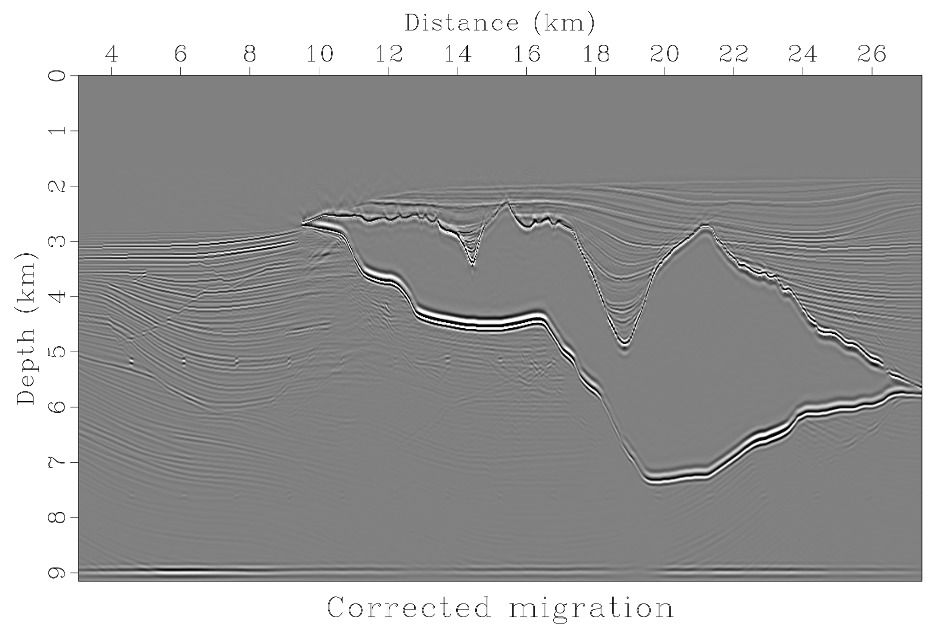

Figure 5.5: The corrected migrated image, found by applying equation (5.10) to $\mathbf{m}_0$. chapter-mighes/sigsbee migdec-shap

We begin with the sub-surface reflectivity model (Figure 5.1(a)) and migration velocity model (Figure 5.1(b)). Next, we forward model the seismic data and migrate it to obtain our first conventionally migrated image, $\mathbf{m}_0$ (Figure 5.2(a)). Then, we forward model $\mathbf{m}_0$ and remigrate that data to obtain $\mathbf{m}_1$ (Figure 5.2(b)). This provides us with the two images, $\mathbf{m}_0$ and $\mathbf{m}_1$, that we can use to find the operation $\mathbf{H}$ that maps $\mathbf{m}_0$ to $\mathbf{m}_1$.

Next, we calculate and apply the data matching operations as described in the previous section. The forward amplitude balancing weight, $\mathbf{A}$, is shown in Figure 5.3(a). The calculated radius for the forward smoothing operation is shown in Figure 5.3(b). After applying these two operators to $\mathbf{m}_0$ as described by equation (5.10), we produce the corrected migrated image, as shown in Figure 5.5. This corrected image better represents the subsurface reflectivity than the conventionally migrated image (Figure 5.2(a)), as it exhibits more correct amplitude content and higher resolution comparable with the reflectivity model.

Figure 5.6 shows a windowed section of the reflectivity model, the conventionally migrated image, and the corrected migrated image. The corrected migrated image exhibits clearly higher resolution and has more correct and consistent amplitude content than the conventionally migrated image.

In addition to directly applying this operator to the conventionally migrated image to improve resolution, this operator can be used as a preconditioner in iterative least-squares migration. In this case, the corrected migrated image could be used as an initial model for least-squares migration for faster convergence.

CONCLUSIONS

Least-squares migration can produce an accurate migrated image, but it is more computationally expensive than conventional migration. In this chapter, we apply an approximate inverse Hessian operator to a conventional migrated image to approximate the least-squares migrated image. Because the primary differences between

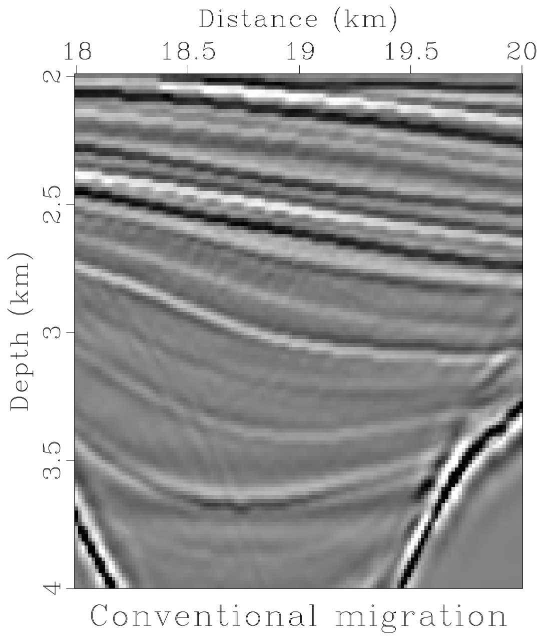

(a)

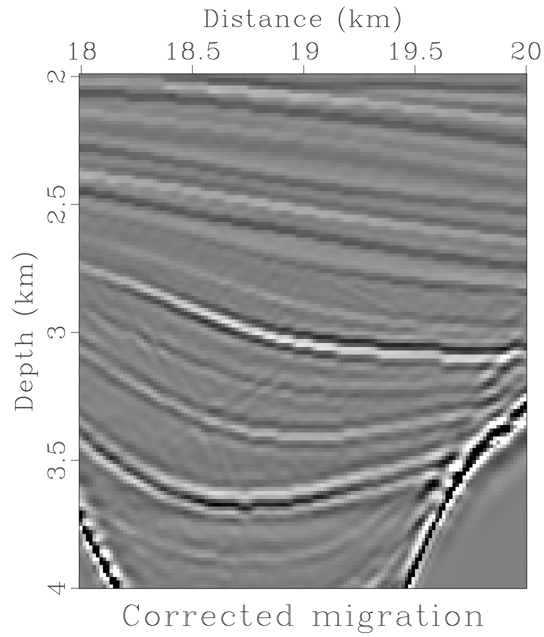

(b)

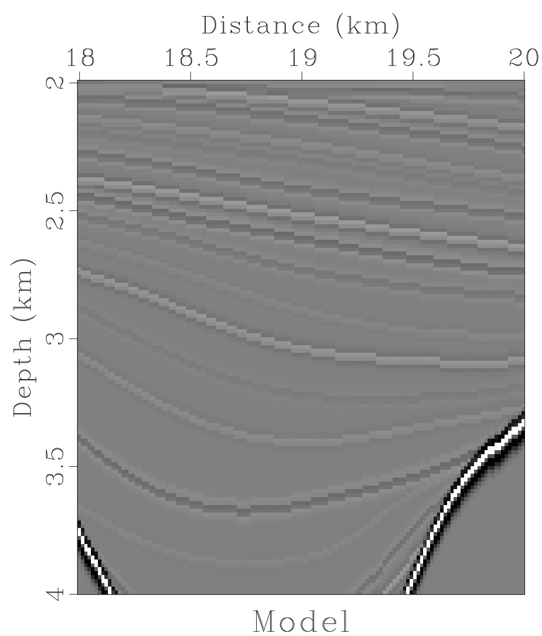

(c)

Figure 5.6: The first migrated image (a), the corrected migrated image (b), and the Sigsbee model reflectivity (c). chapter-mighes/sigsbee image0-w3,migdec-w3,mod-w3

least-squares migration and conventional migration amount to amplitude and frequency variations, we approximate the forward Hessian by calculating frequency and amplitude matching operators. The amplitude matching operator is found by calculating the amplitude envelopes of migrated and remigrated images and smoothly dividing them, and the frequency matching operator is found using an iterative algorithm and non-stationary smoothing. The Hessian is approximated by a combination of these two operators to ensure symmetry. This method involves a windowless approach and is cheap to calculate and apply. Additionally, by defining the Hessian with two separate operators, we can examine, and control, the "ingredients" of the Hessian operator, and see how changing them impacts the final image.

After the forward Hessian is calculated, we invert it iteratively using shaping regularization, and apply it to the conventionally migrated image to get an approximation of the least-squares migrated image. Successful results are achieved on the 2D Sigsbee synthetic model with reverse-time migration as the migration operator.

ACKNOWLEDGMENTS

We thank the sponsors of the Texas Consortium for Computational Seismology (TCCS) for their financial support. The examples in this chapter can be reproduced using the Madagascar open-source software package (Fomel et al., 2013).

Chapter 6

Conclusions

In this thesis, I discussed several methods and applications of data matching in seismic data analysis. Chapter 2 focuses on introducing the three data matching operators that are used in this thesis—shifting, scaling, and filtering. Chapter 3 introduces different methods of frequency balancing using non-stationary smoothing. The first method to find the non-stationary smoothing *radius*, or number of samples each data point is averaged over with a triangle weight, took a theoretical approach based off of the assumption that the data we observe can be modeled by a summation of Ricker wavelets. This method worked well in certain situations, but was not robust enough to work for any given data set. In the second method, I introduced an iterative algorithm to find the smoothing radius, and this method converges quickly and works well in several presented situations. Finally, a modification to this algorithm was shown and allows smoothing for more complex data sets.

This chapter also discusses two applications of these algorithms—the frequency balancing algorithm was demonstrated on an application of matching high-resolution and legacy seismic images, and the modified algorithm was demonstrated on an application of multicomponent seismic image registration.

Chapter 4 goes into more detail of the application of matching and merging high-resolution and legacy seismic images. This example takes two seismic volumes, acquired over the same area but using different technologies, and first matches them before merging them together to produce an optimized third image. First, the method is demonstrated on a 2D line from the Gulf of Mexico. Then, the method is applied to a 3D seismic volume from a different part of the Gulf of Mexico.

Chapter 5 discusses another application of improving migration resolution by approximating the least-squares Hessian using non-stationary data matching operations. An approximation to the least-squares Hessian can be calculated by solving a data matching problem between two conventionally migrated images, and the Hessian can be represented by the combination of amplitude and frequency balancing operations. An example is applied to a 2D synthetic Sigsbee data set.

FUTURE WORK

In the future, the work presented in Chapter 5 should be extended to involve real data and 3D examples. It also could benefit by comparing the results of the proposed approach taken in the chapter to other previous approaches presented to approximate the least-squares Hessian (Hu and Schuster, 1998; Dong et al., 2012; Casasanta et al., 2017; Dai and Schuster, 2013; Sacchi et al., 2007; Aoki and Schuster, 2009; Yu et al., 2006; Hu et al., 2001), to see how it compares in different situations.

Another extension of this data matching procedure may be to incorporate the phase of the signal to be matched. Negligible improvements were made when trying to incorporate phase corrections into the high-resolution and legacy data matching problem of Chapter 4, but other data matching problems could benefit from these corrections.

Several applications of data matching were discussed in this thesis. However, many applications remain unaddressed from a data matching standpoint. Problems such as seismic and well-log tying, deconvolution, automatic gain control (AGC), and surface-related multiple elimination (SRME) can also be recast as data matching problems. Looking at these problems in a new light may bring advancements to computational geophysics.

Appendix

CODE

The examples in this thesis were implemented with the Madagascar open-source software environment for reproducible computational experiments (Fomel et al., 2013). The package is available at `http://www.ahay.org/`.

The reproducible document for the results in this thesis, including code, is available at `http://www.sygreer.com/research/honorsThesis`. However, some of the data used in this thesis are proprietary, so those results may not directly be reproducible.

For brevity in this thesis, code is only included for one example of the main frequency balancing algorithm presented in Chapter 3. The code for the rest of the examples in this thesis are available online at the URL above.

Table 1: List of figures in this thesis and the locations of scripts and programs to generate them

Figures	**Directory**	**Listings**
2.1	chapter-locfreq/merge/	1, 2, 3
2.2, 2.3	chapter-background/dmExample/	—
3.1, 3.2, 3.3, 3.4	chapter-merge/apache/	—
3.5, 3.6, 3.7, 3.8	chapter-locfreq/merge/	1, 2, 3
3.9, 3.10	chapter-locfreq/vecta/	—
3.11	chapter-locfreq/convergence/	—
4.1, 4.2, 4.3, 4.4	chapter-merge/apache/	—
4.5, 4.6	chapter-merge/pcable/	—
4.7	chapter-merge/pcable2/	—
5.1, 5.2, 5.3, 5.5, 5.6	chapter-merge/mighes/	—
5.4,	chapter-merge/triop/	—

Listing 1: chapter-locfreq/merge/SConstruct

```
from rsf.proj import *
from radius import radius

# must have 'legacy.rsf' and 'hires.rsf' initial data sets in same directory

# Initial figures
```

```
Result('legacy','grey title="Legacy"')
Result('hires-agc','hires',
       'agc rect1=2000 rect2=5 | grey title="High-resolution"')

# frequency content
Flow('legacy-spec','legacy','spectra all=y')
Result('nspectra-orig','high-spec legacy-spec',
     '''cat axis=2 ${SOURCES[1]} | scale axis=1 | window max1=180 |
        graph title="Normalized Spectra" label2="Amplitude" unit2=""''')

# Balance local frequency
flol=40
corrections = 5
Flow('legacyfilt','legacy','bandpass flo=%d '%(flol))
radius('hires','legacyfilt', corrections, [0.13,0.2,0.3,0.5,0.5],
       bias=0, clip=90, rect1=80, rect2=16, maxval=90 )

End()
```

Listing 2: chapter-locfreq/merge/radius.py

```
from rsf.proj import *

def radius(high, low,               # initial high and low frequency images
           niter,                   # number of corrections
           c,                       # 'step length' for radius corrections. Can
                                    #       be type int or float for constant c
                                    #       or type array for changing c.
           bias=-15, clip=30,       # bias and clip for display
           rect1=40, rect2=80,      # radius for local frequency calculation
           maxrad=1000,             # maximum allowed radius
           theor=True,              # use theoretical smoothing radius
           scale=9,                 # scale for theoretical smoothing radius
           initial=10,              # initial value for contant smoothing radius
           minval=0, maxval=25,     # min and max local frequency for display
           titlehigh="Hires",
           titlelow="Legacy"):

    if type(c) is float or type(c) is int:
        c = [c]*niter

    # plot image
    def seisplot(name):
        return 'grey title="%s"'%name

    # local frequency
    locfreq = '''iphase order=10 rect1=%d rect2=%d hertz=y complex=y |
                 put label="Frequency" unit=Hz'''%(rect1,rect2)

    def locfreqplot(name):
        return 'grey mean=y color=j scalebar=y title="%s" '%name

    # difference in local frequencies
    freqdif = 'add scale=-1,1 ${SOURCES[1]} | put label=Frequency'

    def freqdifplot(num):
        return '''grey allpos=y color=j scalebar=y mean=y
                  title="Difference in Local Frequencies %s"
                  clip=%d bias=%d minval=%d
                  maxval=%d''' %(num,clip,bias,minval,maxval)

```

```
# plot spectral content
specplot = '''cat axis=2 ${SOURCES[1]} |
             scale axis=1 | window max1=180 |
             graph title="Normalized Spectra" label2="Amplitude" unit2=""'''

# plot smothing radius
def rectplot(name):
    return '''grey color=j mean=y title="%s" scalebar=y barlabel=Radius
              barunit=samples'''%name

# smooth with radius
smooth = 'nsmooth1 rect=${SOURCES[1]}'

############################################################################

# plot images
Result(high, seisplot(titlehigh))
Result(low, seisplot(titlelow))

# initial local frequency
Flow('high-freq',high,locfreq)
Result('high-freq',locfreqplot('%s Local Frequency'%titlehigh))

Flow('low-freq',low,locfreq)
Result('low-freq',locfreqplot('%s Local Frequency'%titlelow))

# initial difference in local frequency
Flow('freqdif','low-freq high-freq',freqdif)
Result('freqdif',freqdifplot(''))

# initial smoothing radius
if (theor):
    from math import pi
    Flow('rect0','low-freq high-freq','''math f1=${SOURCES[1]}
    output="sqrt(%g*(1/(input*input)-1/(f1*f1)))/%g"'''%(scale,2*pi*0.001))
else:
    Flow('rect0','low-freq','math output=%f'%initial)

Result('rect0',rectplot("Smoothing Radius 0"))

# smoothing using intial smoothing radius guess
Flow('high-smooth0','%s rect0' % high,smooth)
Result('high-smooth0', seisplot("%s Smooth 0"%titlehigh))

# frequency spectra
Flow('high-spec',high,'spectra all=y')
Flow('low-spec',low,'spectra all=y')
Flow('high-smooth-spec0','high-smooth0','spectra all=y')
Result('nspectra','high-spec low-spec',specplot)
Result('high-smooth-spec0','high-smooth-spec0 low-spec',specplot)

Flow('high-smooth-freq0','high-smooth0',locfreq)
Result('high-smooth-freq0',
       locfreqplot("%s Local Frequency Smoothed %d" %(titlehigh,0)))

Flow('freqdif-filt0','low-freq high-smooth-freq0',freqdif)
Result('freqdif-filt0',freqdifplot('0'))

prog=Program('radius.c')
for i in range(1, niter+1):
    j = i-1
```

```
        # update smoothing radius
        Flow('rect%d'%i,'rect%d freqdif-filt%d %s'%(j,j,prog[0]),
             './${SOURCES[2]} freq=${SOURCES[1]} c=%f'%c[j])
        Result('rect%d'%i,rectplot("Smoothing Radius %d")%i)

        # smooth image with radius
        Flow('high-smooth%d'%i,'%s rect%d'%(high,i),smooth)
        Result('high-smooth%d'%i, seisplot('%s Smooth %d'%(titlehigh,i)))

        # smoothed spectra
        Flow('high-smooth-spec%d'%i,'high-smooth%d'%i,'spectra all=y')
        Result('high-smooth-spec%d'%i,'high-smooth-spec%d low-spec'%i,specplot)

        # smoothed local frequency
        Flow('high-smooth-freq%d'%i,'high-smooth%d'%i,locfreq)
        Result('high-smooth-freq%d'%i,
               locfreqplot('%s Local Frequency Smoothed %d'%(titlehigh,i)))

        # frequency residual
        Flow('freqdif-filt%d'%i,'low-freq high-smooth-freq%d'%i,freqdif)
        Result('freqdif-filt%d'%i,freqdifplot(str(i)))
```

Listing 3: chapter-locfreq/merge/radius.c

```
/* smoothing radius (min = 1) */
#include <rsf.h>
#include <math.h>

int main (int argc, char* argv[])
{
    int n1, n1f, n2, n2f, i, n12, n12f;
    float *rect, *fr, maxrad, c, *rad;
    sf_file in, out, freq;

    sf_init (argc,argv);

    in = sf_input("in");
    freq = sf_input("freq");
    out = sf_output("out");

    if (!sf_histint(in,"n1",&n1)) sf_error("No n1= in input.");
    if (!sf_histint(freq,"n1",&n1f)) sf_error("No n1= in frequency difference.");

    n2 = sf_leftsize(in,1);
    n2f = sf_leftsize(freq,1);

    n12 = n1*n2;
    n12f = n1f*n2f;

    if (n1 != n1f) sf_error("Need matching n1");
    if (n2 != n2f) sf_error("Need matching n2");

    if (!sf_getfloat("c",&c)) c=1.;
    if (!sf_getfloat("maxrad",&maxrad)) maxrad=1000.;

    rect = sf_floatalloc(n12);
    sf_floatread(rect,n12,in);

    fr = sf_floatalloc(n12f);
    sf_floatread(fr,n12,freq);
```

```
    rad = sf_floatalloc(n12);

    for (i=0; i < n12; i++) {

        /* update radius */
      rad[i] = rect[i]+c*fr[i];

        /* set constraint conditions: [1, maxrad] */
        if (rad[i] > maxrad)
                rad[i] = maxrad;
        if (rad[i] < 1.0)
                rad[i] = 1.0;
    }

    sf_floatwrite(rad,n12,out);
    exit(0);
}
```

Bibliography

Al-Inaizi, S., R. Bridle, and N. Nakhla, 2004, Comparison of pre and post-stack supermerge of ten 3D blocks: Presented at the 74th Annual International Meeting, SEG, Expanded Abstracts, Society of Exploration Geophysicists.

Aoki, N., and G. T. Schuster, 2009, Fast least-squares migration with a deblurring filter: GEOPHYSICS, **74**, WCA83–WCA93.

Bader, S., X. Wu, and S. Fomel, 2018, Missing log data interpolation and semiautomatic seismic well ties using data matching techniques: Interpretation. (Submitted).

Carter, D., and S. Pambayuning, 2009, Extended bandwidth by a frequency domain merge of two 3D seismic volumes: The Leading Edge, **28**, 386–386.

Casasanta, L., F. Perrone, G. Roberts, A. Ratcliffe, K. Purcell, A. Jafargandomi, and G. Poole, 2017, Applications of single-iteration Kirchhoff least-squares migration: Presented at the 87th Annual International Meeting, SEG, Expanded Abstracts, Society of Exploration Geophysicists.

Claerbout, J. F., 1992, Earth Soundings Analysis: Processing Versus Inversion: Blackwell Scientific Publications.

Dai, W., and G. T. Schuster, 2013, Plane-wave least-squares reverse-time migration: GEOPHYSICS, **78**, S165–S177.

Dong, S., J. Cai, M. Guo, S. Suh, Z. Zhang, B. Wang, and Z. Li, 2012, Least-squares reverse time migration: towards true amplitude imaging and improving the resolution: Presented at the 82nd Annual International Meeting, SEG, Expanded Abstracts, Society of Exploration Geophysicists.

Dutta, G., Y. Huang, W. Dai, X. Wang, and G. T. Schuster, 2014, Making the most out of the least (squares migration): 84th Annual International Meeting, SEG, Expanded Abstracts, 4405–4410.

Fomel, S., 2007a, Local seismic attributes: GEOPHYSICS, **72**, A29–A33.

———, 2007b, Shaping regularization in geophysical-estimation problems: GEOPHYSICS, **72**, R29–R36.

Fomel, S., M. Backus, K. Fouad, B. Hardage, and G. Winters, 2005, A multistep approach to multicomponent seismic image registration with application to a West Texas carbonate reservoir study: 75th Ann. Internat. Mtg, Soc. of Expl. Geophys., 1018–1021.

Fomel, S., and M. M. Backus, 2003a, Multicomponent seismic data registration by least squares: Presented at the 73rd Annual International Meeting, SEG, Expanded Abstracts, Society of Exploration Geophysicists.

———, 2003b, Multicomponent seismic data registration by least squares: 73rd Annual International Meeting, Soc. of Expl. Geophys., 701–784.

Fomel, S., and L. Jin, 2009, Time-lapse image registration using the local similarity attribute: GEOPHYSICS, **74**, A7–A11.

Fomel, S., P. Sava, I. Vlad, Y. Liu, and V. Bashkardin, 2013, Madagascar: open-source software project for multidimensional data analysis and reproducible computational experiments: Journal of Open Research Software, **1**, e8.

Gholamy, A., and V. Kreinovich, 2014, Why ricker wavelets are successful in processing seismic data: Towards a theoretical explanation: Presented at the 2014 IEEE Symposium on Computational Intelligence for Engineering Solutions (CIES), IEEE.

Greer, S., and S. Fomel, 2017a, Balancing local frequency content in seismic data using non-stationary smoothing: , Society of Exploration Geophysicists, 4278 – 4282.

———, 2017b, Matching and merging high-resolution and legacy seismic images: , Society of Exploration Geophysicists, 5933 – 5937.

———, 2018, Matching and merging high-resolution and legacy seismic images: GEOPHYSICS, **83**, V115–V122.

Greer, S., Z. Xue, and S. Fomel, 2018, Improving migration resolution by approximating the least-squares hessian using non-stationary amplitude and frequency matching: Presented at the 88th Annual International Meeting, SEG, Expanded Abstracts, Society of Exploration Geophysicists. (Submitted).

Guitton, A., 2004, Amplitude and kinematic corrections of migrated images for nonunitary imaging operators: GEOPHYSICS, **69**, 1017–1024.

———, 2017, Fast 3D least-squares RTM by preconditioning with nonstationary matching filters: Presented at the 87th Annual International Meeting, SEG, Expanded Abstracts, Society of Exploration Geophysicists.

Hale, D., 2013, Dynamic warping of seismic images: GEOPHYSICS, **78**, S105–S115.

Hardage, B. A., M. V. DeAngelo, P. E. Murray, and D. Sava, 2011, Multicomponent seismic technology: Society of Exploration Geophysicists.

Herrera, R. H., S. Fomel, and M. van der Baan, 2014, Automatic approaches for seismic to well tying: Interpretation, **2**, SD9–SD17.

Herrera, R. H., and M. van der Baan, 2012, Guided seismic-to-well tying based on dynamic time warping: 82nd Annual International Meeting, Society of Exploration Geophysicists, 1–5.

Hestenes, M. R., and E. Stiefel, 1952, Methods of Conjugate Gradients for Solving

Linear Systems: Journal of Research of the National Bureau of Standards, **49**, 409–436.

Hou, J., and W. Symes, 2016, Accelerating least squares migration with weighted conjugate gradient iteration: Presented at the 78th EAGE Conference and Exhibition 2016, EAGE Publications BV.

Hou, J., and W. W. Symes, 2015, An approximate inverse to the extended born modeling operator: GEOPHYSICS, **80**, R331–R349.

Hu, J., and G. T. Schuster, 1998, Migration deconvolution: Presented at the Mathematical Methods in Geophysical Imaging V, SPIE.

Hu, J., G. T. Schuster, and P. A. Valasek, 2001, Poststack migration deconvolution: GEOPHYSICS, **66**, 939–952.

Kuehl, H., and M. D. Sacchi, 2003, Least-squares wave-equation migration for AVP/AVA inversion: GEOPHYSICS, **68**, 262–273.

Liu, Y., and S. Fomel, 2012, Seismic data analysis using local time-frequency decomposition: Geophysical Prospecting, **61**, 516–525.

Lumley, D., D. C. Adams, M. Meadows, S. Cole, and R. Wright, 2003, 4D seismic data processing issues and examples: 73rd Annual International Meeting, Society of Exploration Geophysicists, 1394–1397.

Meckel, T., N. L. Bangs, and T. Hess, 2017, 3D multichannel seismic field data from the San Luis Pass region off Galveston, Texas, acquired by the R/V Brooks-McCall in 2013 (BM1310).

Meckel, T. A., and F. J. Mulcahy, 2016, Use of novel high-resolution 3D marine seismic technology to evaluate Quaternary fluvial valley development and geologic controls on shallow gas distribution, inner shelf, Gulf of Mexico: Interpretation, **4**, SC35–SC49.

Mohan, T. R. M., C. B. Yadava, S. Kumar, K. K. Mishra, and K. Niyogi, 2007, Prestack merging of land 3D vintages — a case history from Kavery Basin, India: Presented at the 77th Annual International Meeting, SEG, Expanded Abstracts, Society of Exploration Geophysicists.

Müller, M., 2007, Dynamic time warping, *in* Information Retrieval for Music and Motion: Springer Berlin Heidelberg, 69–84.

Paffenholz, J., B. McLain, J. Zaske, and P. Keliher, 2002, Subsalt multiple attenuation and imaging: Observations from the Sigsbee2B synthetic dataset: 72nd Annual International Meeting, SEG, Expanded Abstracts, 2122–2125.

Petersen, C. J., S. Buenz, S. Hustoft, J. Mienert, and D. Klaeschen, 2010, High-resolution P-Cable 3D seismic imaging of gas chimney structures in gas hydrated sediments of an Arctic sediment drift: Marine and Petroleum Geology, **27**, 19811994.

Phillips, M., and S. Fomel, 2016, Seismic time-lapse image registration using amplitude-adjusted plane-wave destruction: 86th Annual International Meeting, SEG, Expanded Abstracts, Society of Exploration Geophysicists, 5473–5478.

Rickett, J. E., 2003, Illumination-based normalization for wave-equation depth migration: GEOPHYSICS, **68**, 1371–1379.

Ross, C. P., and M. S. Altan, 1997, Time-lapse seismic monitoring: Some shortcomings in nonuniform processing: The Leading Edge, **16**, 931–937.

Sacchi, M. D., J. Wang, and H. Kuehl, 2007, Estimation of the diagonal of the migration blurring kernel through a stochastic approximation: Presented at the 77th Annual International Meeting, SEG, Expanded Abstracts, Society of Exploration Geophysicists.

Schuster, G. T., 2017, Seismic inversion: Society of Exploration Geophysicists.

Tsinaslanidis, P., A. Alexandridis, A. Zapranis, and E. Livanis, 2014, Dynamic time warping as a similarity measure: Applications in finance: Presented at the Hellenic Finance and Accounting Association.

Ursenbach, C., P. Cary, and M. Perz, 2013, Limits on resolution enhancement for PS data mapped to PP time: The Leading Edge, **32**, 64–71.

White, R. E., 1991, Properties of instantaneous seismic attributes: The Leading Edge, **10**, 26–32.

Xue, Z., Y. Chen, S. Fomel, and J. Sun, 2016, Seismic imaging of incomplete data and simultaneous-source data using least-squares reverse-time migration with shaping regularization: GEOPHYSICS, **81**, no. 1, S11–S20.

Yu, J., J. Hu, G. T. Schuster, and R. Estill, 2006, Prestack migration deconvolution: GEOPHYSICS, **71**, S53–S62.

Zhou, J., J. Sun, and X. Ma, 2014, Application of Gabor transform to amplitude spectrum matching for merging seismic surveys: Presented at the 84th Annual International Meeting, SEG, Expanded Abstracts, Society of Exploration Geophysicists.

Vita

Sarah graduated with high honors from Cinco Ranch High School in Katy, Texas in 2014 and came to The University of Texas at Austin to pursue her undergraduate studies. She is a candidate for a Bachelor of Science degree in Geophysics from the Jackson School of Geosciences and a Bachelor of Science degree in Mathematics from the College of Natural Sciences. After graduation, she plans on pursuing a PhD in Mathematics and Computational Science at the Massachusetts Institute of Technology.

Permanent address: 2175 Stonecrest Drive, Eugene, OR, 97401, USA

This thesis was typeset with LaTeX† by the author.

†LaTeX is a document preparation system developed by Leslie Lamport as a special version of Donald Knuth's TeX Program.